The Whitehill Formation – a high conductivity marker horizon in the Karoo Basin

Thomas Branch
GeoForschungsZentrum Potsdam, Telegrafenberg, 14473 Potsdam, Germany
AEON-Africa Earth Observatory Network and Department of Geological Sciences,
University of Cape Town, Rondebosch 7700, South Africa.
e-mail: tbranch@geology.uct.ac.za

Oliver Ritter
GeoForschungsZentrum Potsdam, Telegrafenberg, 14473 Potsdam, Germany
e-mail: oritter@gfz-pozsdam.de (corresponding author)

Ute Weckmann
GeoForschungsZentrum Potsdam, Telegrafenberg, 14473 Potsdam, Germany
Universität Potsdam, Institut für Geowissenschaften, Karl-Liebknecht-Strasse 24, 14476 Potsdam, Germany
e-mail: uweck@gfz-pozsdam.de

Reinhard F. Sachsenhofer
Geologie und Lagerstättenlehre am Department Angewandte Geowissenschaften und Geophysik,
Montanuniversität, A-8700 Leoben, Austria
e-mail: reinhard.sachsenhofer@mu-leoben.at

Frank Schilling
GeoForschungsZentrum Potsdam, Telegrafenberg, 14473 Potsdam, Germany
e-mail: fsch@gfz-pozsdam.de

ABSTRACT

Within the Inkaba yeAfrica project, magnetotelluric (MT) data were acquired along three profiles across the Karoo Basin in South Africa. The entire Karoo Basin and its sedimentary sequences are intersected by a number of deep boreholes, which were drilled during exploration for coal, oil and uranium. One of the most consistent and prominent features in the electrical conductivity images is a shallow, regionally continuous, sub-horizontal band of high conductivity that seems to correlate with the Whitehill Formation. The Whitehill Formation in particular is known to be regionally persistent in composition and thickness and can be traced throughout the entire Karoo Basin. In the region of our experiments, the Whitehill Formation varies in thickness between 50 to 70 m and consists of pyritic black shales with up to 14 weight % carbonaceous matter. Rocks can exhibit high electrical conductivity if electronically conducting minerals, such as graphite, are interconnected. To study physical properties and the maturity of the carbon present in the Whitehill Formation, impedance spectroscopy and vitrinite reflectance were applied to core samples from the SA1/66 borehole, taken from this formation at a depth range between 2750 m and 2800 m. Vitrinite reflectance analysis of the pseudo-coal and oil shale rocks indicates that most of the carbon is in the meta-anthracite maturity field, approaching, in one sample, the "graphite window". Impedance spectroscopy reveals that the highest electrical conductivities are associated with the pyrite rich portion of one sample, showing conductivities well above 1 S/m. Recordings on pyrite-poor samples are less conclusive, with observed conductivities varying in the range of a few S/m to mS/m. Measurements on samples from the Whilehill Formation, on the other hand, show consistently low resistivities in the range between 4 to 6 Ωm. This result suggests strongly that the sub-horizontal conductivity anomaly in the MT models is linked with the carbon-rich sequences of the Whitehill Formation

Introduction

High electrical conductivity for the Whitehill Formation of the Lower Karoo Supergroup was first identified by in situ borehole measurements during SOEKOR's regional oil exploration program in the 1960's (Cole and McLachlan, 1994). Recently Van Zijl (2006) reviewed the results of some 280 deep DC electrical soundings that were conducted between 1966 and 1980 in the Karoo Basin. Most of the sedimentary or meta-sedimentary rocks of the upper Karoo are associated with resistivities in the order of a few hundred Ωm. At some locations, however, the DC sounding curves indicate a significant drop in the apparent resistivity curves for very long electrode separations (AB/2 > 10 km). From these curves, Van Zijl (2006) estimated resistivities as low as 1 Ωm on average and associated these zones to high conductivities of the Whitehill Formation within the Karoo sedimentary basin. A much deeper high

doi:10.2113/gssajg.110.2-3.465

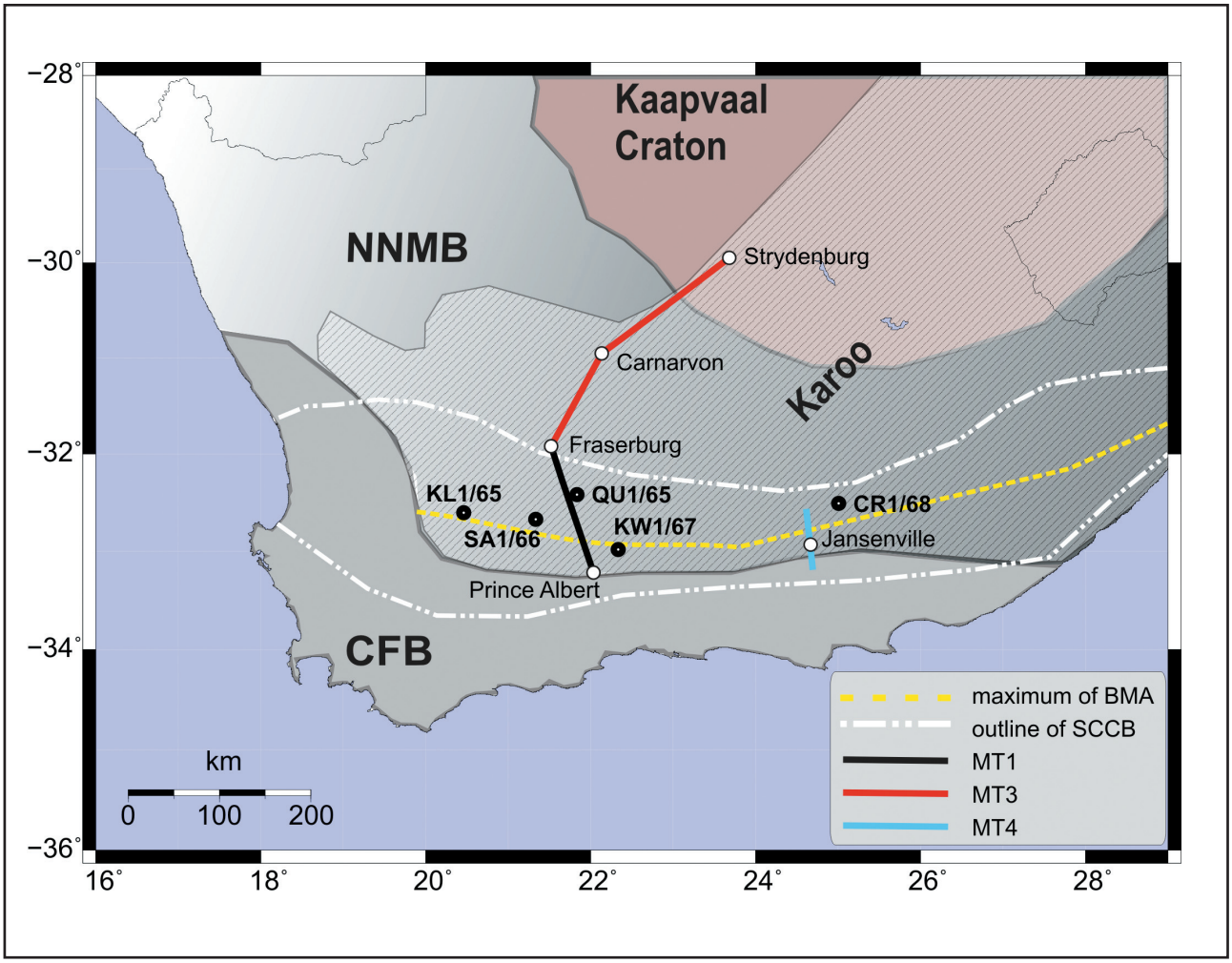

Figure 1. The MT profiles cross the entire Karoo Basin (hatched). Profile MT1 (black line) starts at Prince Albert and extends northwards away from the exposed Cape Fold Belt across the Great Karoo to Fraserburg. The northern profile segment MT3 (red line) extends in northeast direction from Fraserberg onto the Kaapval Craton. Profiles MT1 and MT4 (blue line) cross the centre of the Beattie Magnetic Anomaly (BMA) and the Southern Cape Conductive Belt (SCCB). SA1/66 indicates the location of the deep borehole from which the rock samples for this investigation were obtained. KL1/65, QU1/65, KW1/67, and CR1/68 mark positions of other boreholes discussed in the text. CFB – Cape Fold Belt; NNMB – Namaqua Natal Mobile Belt; BMA – Beattie Magnetic Anomaly.

conductivity zone in South Africa was identified by Gough *at al.* (1973) with magnetometer array studies, the so-called Southern Cape Conductive Belt (SCCB). The location of the east to west striking (SCCB) was inferred from a reversal of induction vectors for very large penetration depths. The anomalous high conductivity zone seems to be situated in the lower crust of the Namaqua Natal Mobile Belt (NNMB) with an approximate width of 200 km.

More recently, between 2004 and 2006 high-resolution magnetotelluric (MT) profiles were completed in the southern Karoo. The MT profiles cross the Karoo Basin in the NNMB (Figure 1). In the south, starting at Prince Albert, the profile extends northwards across the Great Karoo to Fraserburg which is situated on top of the Great Escarpment. From Fraserburg, the profile continues north-eastwards onto the Kaapvaal craton. The surveys are part of the *Inkaba yeAfrica* project and specifically targeted the conductive nature of the SCCB along with the collinear Beattie Magnetic Anomaly (BMA) (Weckmann *et al.*, 2007a). The BMA was also the target of an additional 70 km long profile (MT4), 350 km farther east (see also Weckmann *et al.*, 2007b).

One of the most prominent and consistent features in the MT data is a continuous, near-horizontal conductor at shallow crustal depths (above 6 km). With the much larger sounding depths of MT when compared with DC methods, this formation can be identified more clearly. It is also possible to trace this layer over very large distances in the east and north directions.

On the basis of these new MT data, we discuss the observed high conductivities in the shallow crust in view of results from laboratory measurements on rock samples from the Whitehill and underlying formations. Hand samples were obtained from borehole SA1/66, 50 km to the west of the MT profiles, at depths that correlate with the conductor in the MT model. These samples were attained from the South African Borehole Library in Pretoria. At the GeoForschungsZentrum, their electrical conductivity was determined using impedance

spectroscopy. Vitrinite reflectance analysis, carried out at the Montanuniversität in Leoben, was used to examine the possible relation to carbon maturation.

Geological Setting

The Karoo Supergroup of late Carboniferous to Middle Jurassic age was formed in the great Gondwana basin and hosts all of South Africa's coal deposits (Snyman, 1998). Described as a polyphase, retro-arc foreland basin (Cole, 1992; Johnson *et al*., 1996) the Karoo Basin experienced episodic tectonic uplift as well as lithospheric sag largely associated with subduction of the palaeopacific plate to the south at ~292 Ma (Cole, 1992). The foreland load associated with this subduction influenced the deposition of the Lower Karoo's glacigenic Dwyka Group and then its transgressive, carbon-rich Prince Albert and Whitehill Formations over the upper sequences of the Cape Basin (Table 1). With a sediment provenance in the cratonic hinterland to the north, deposition of these sequences was on a horizontal shelf within a brackish, shallow sea of depths between 50 to 150 m (Cole and McLachlan, 1994). At this time the Karoo Basin extended into South America where the Prince Albert and Whitehill Formation are known as the Piedra Azul and Irati Formations, respectively (Lopez-Gamudi and Rossello, 1998).

Before the end of the Karoo Basin's deposition, which culminated with the extrusion of the Drakensberg Basalts, four major Cape Fold Belt (CBF) tectonic paroxysms took place at ~278, ~258, ~247 and ~230 Ma involving the Cape and Karoo Supergroups (Halbich, 1992). However, isopach data for the Whitehill Formation indicate thinning over major syntaxial anticlinoria within the Cape Syntaxis. This suggests that these anticlinoria must have already experienced some surface expression during the Whitehill Formation's deposition (de Beer, 1982; Cole and McLachlan, 1994). By the end of the CFB's last paroxysm, soft-sediment deformation and movement along southward dipping decollements resulted in major northward-directed overthrusts and folding with duplication of the Karoo sequences in the eastern basin (Newton, 1992).

Compositions of the Whitehill and Price Albert Formations

The Whitehill Formation, formerly known as the White Band, consists of black, carbonaceous shales with intermittent chert lenses and pyritic stringers; the latter rarely exceeding 20 mm in thickness. The sedimentary structure is generally massive, however laminations do occur that resemble algal lamellae. The formation appears white due to weathering of pyrite (sulphide) at surface to sulfate (gypsum) (de Wit, personal communication, 2007).

The boundary between the Whitehill Formation and the post-glacial Prince Albert Formation is often a gradational lithological change; this is also true for the organic carbon and pyrite content. Consequently, low resistivities in the order of those for the Whitehill Formation have also been recorded for the Prince Albert Formation in situ for borehole KW1/67 situated less than 50 km east of the MT profile (SOEKOR KW1/67). The Prince Albert Formation's lithology is more dominated by fine-grained siltstones and sandstones. Above the Whitehill Formation sequences grade vertically upwards into the sandier Upper Ecca Group which coincides with the CFB's second major paroxysm

Table 1. Summary of stratigraphy and lithologies discussed in the paper (modified after Catuneau, 2004; Milani and de Wit, 2007). Bold vertical line indicates range of intermittent tectonic activity within the Cape Fold Belt (after Halbich *et al*., 1983).

Supergroup	Group/Formation			Age	SA1/66 Borehole Intercept	Basin Evolution
Karoo Supergroup	Beaufort Group			>258-228 Ma	457 m	Fluvial accumulation
	Ecca Group	Upper Ecca			1280 m	Turbidite influx (from south)
		Lower Ecca	Collingham Fm.	270-276 Ma	2743 m	
			Whitehill Fm.		2790 m	Lacustrine deposition
			Prince Albert Fm.		2842 m	Post-Glacial marine transgression
	Dwyka Group			289 Ma 342 Ma	(*borehole ends in Dwyka)* 3100 m	Glacial Diamictites
Local Unconformity/disconformity						
Cape Supergroup				~500Ma		Local glacial diamictites top of Witteberg Group Extension and thermal subsidence of Cape Basin

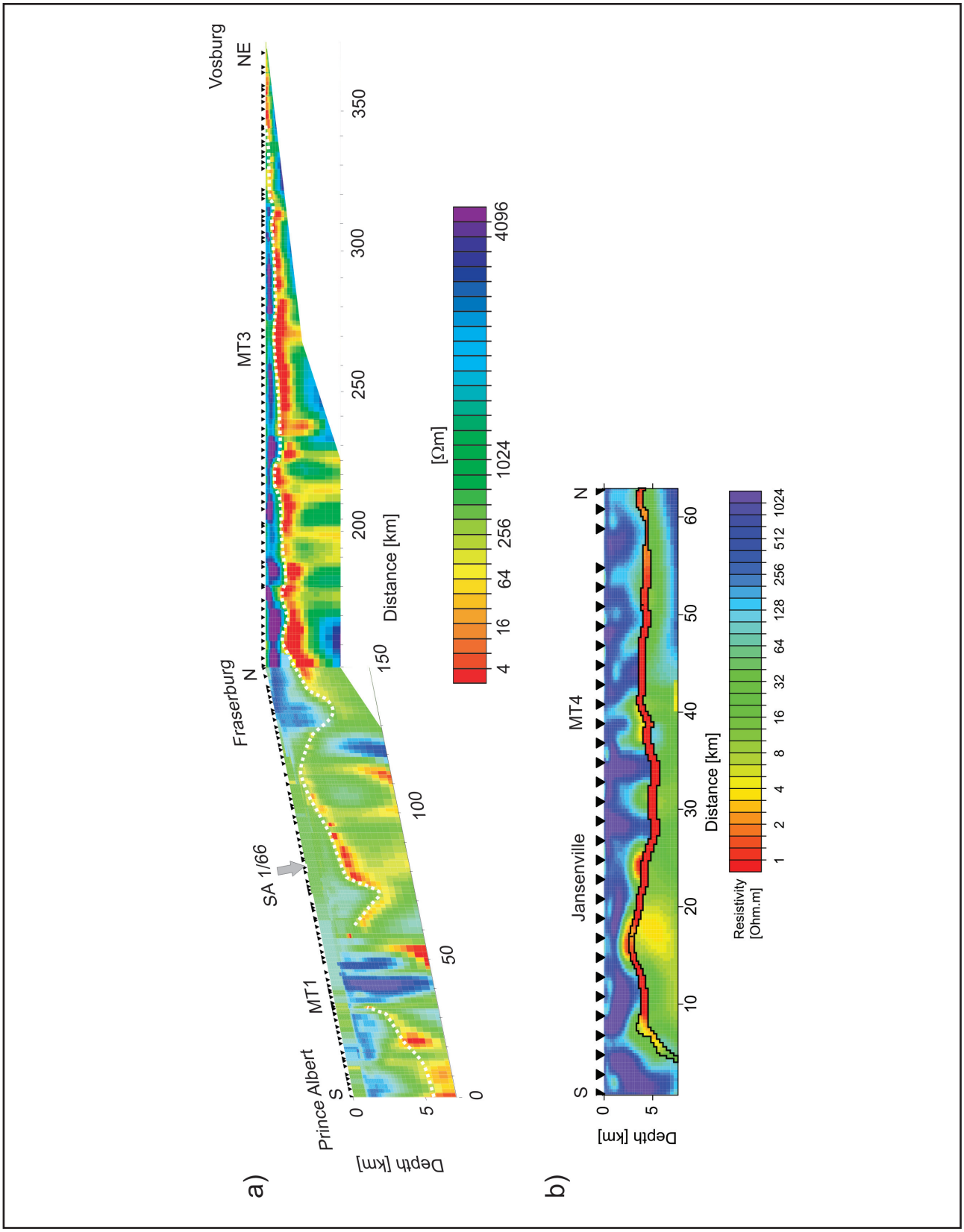

Figure 2. Electrical resistivity distribution in the upper crust derived from 2D inversion of magnetotelluric data acquired along (**a**) profiles MT1 and MT3 and (**b**) profile MT4; see Figure 1 for profile locations. Red and yellow colours mark regions of high electrical conductivity (low resistivity). The dotted line in a) indicates the top of a highly conductive, sub-horizontal layer which likely extends throughout the entire Karoo Basin. The image in (b) is derived from a different 2D inversion strategy (Weckmann *et al.*, 2007b, this issue) using data from MT4, 350 km farther to the east. It is very likely that all of the upper-crustal, high conductivity zones revealed in the MT models are caused by the carbon-rich sequences of the Whitehill Formation (see text). It is at least conceivable that the high conductive band is laterally continuous between the two regions. The location of borehole SA1/66 is projected onto profile MT1 for comparison.

characterized by deeper water conditions, submarine fan deposits and distal turbidites (Cole, 1992).

Maximum C_{Org} values of 7.9% and 5.1% for the Collingham Formation (above the Whitehill Formation) and Prince Albert Formation (below the Whitehill Formation) respectively have been reported by Cole and McLachlan (1994). However, C_{Org} contents are consistently higher for the Whitehill Formation and this is especially the case for boreholes proximal to the MT profiles (such as QU1/65 and KL1/65) with a C_{Org} maximum of 14.8% and 8.1% respectively. In general, the southernmost basin had a 3.0% higher C_{Org} content than samples from the north of the basin; this is largely due to gasification effects from the doleritic dike swarms in the north (Cole and McLachlan, 1994).

The entire Lower Karoo sequence has pervasive pyritic stringers, yet these become distinctly more common as one stratigraphically approaches the Whitehill Formation (Cole and McLachlan, 1994; SOEKOR KW 1/67). In borehole CR1/68, some 400 km to the east of profile MT1 and in the vicinity of profile MT4, between the depths of 3670 m to 3717 m, pyrite reaches a rock average of 10% (SOEKOR CR 1/68). Carbonaceous stringers containing pyrite crystals are found in several boreholes (Cole and McLachlan, 1994).

Metamorphic grade for the Karoo Basin increases from un-metamorphosed to lower anchi-grade (150° C / 3.5 kbar) in the north to epizonal (350° C / 2.5 kbar) adjacent to the CFB in the south (Halbich, 1983). This includes four types of metamorphism: burial, dynamo-thermal (related the CFB), contact (from dolerite swarms in the north), and hydrothermal (related to the extrusion of the Drakensberg basalts). Rocks in the tectonic transition in the frontal ranges of the Cape Fold Belt zone have undergone significant deformation (Craddock *et al.,* 2007). Regional fluid inclusion analyses on quartz and calcite from syntectonic veins revealed temperatures between 150 to 200°C and pressures between 1 and 2 kbar during the peak of deformation for this region (Egle, 1996; Egle *et al.*, 1998). For carbonaceous horizons this resulted in maturation of organic matter and the formation of coal. Contact metamorphism from pervasive doleritic intrusions which were contemporaneous with the Drakensberg flood basalts, along with a lack of reservoirs for the Karoo Basin, ultimately destroyed the Whitehill Formation's petroleum potential (Cole and McLachlan, 1994).

Magnetotelluric data

From 2004 to 2006, MT data was recorded in three experiments along four profiles crossing the Karoo Basin. Profiles MT1 and MT3 (Figure 1) followed the major Agulhas-Karoo transect of the Inkaba yeAfrica project and covered a section from Prince Albert to Fraserburg (MT1), crossing the BMA and the SCCB, and further on towards Strydenberg (MT3). The 70 km long profile MT4 is centred on Jansenville, 350 km farther east (see Weckmann *et al.*, 2007b, this issue). Natural electromagnetic field variations were recorded with a site spacing of 2-3 km in a period range from 0.001 s – 1000 s along all profiles. Data analysis and interpretation of profile MT1 are described in detail in Weckmann *et al.* (2007a) and in Weckmann *et al.* (2007b, this issue) for MT4. Figure 2 shows an image of the subsurface electrical conductivity distribution of the upper 5 to 7 km across the entire Karoo Basin. The section following MT1 is taken from a 2D inversion model presented in Weckmann *et al.* (2007a). The north-eastward extension along MT3 is a 2D inversion result using only the short period data (0.01 s to 1 s) from preliminary (in-field) processing. The restriction to a smaller period band is necessary as most of the longer period data require re-processing (using a remote reference) to increase data quality in the so-called dead band at around 10 s. Strike and dimensionality analysis for the short period data reveals a predominantly layered (1D) conductivity distribution. This is consistent with the geological setting of sub-horizontal layering of the Karoo sediments in the upper crust (< ~5 km). At periods >1 s, the longest periods of our analysis, the data show a more pronounced strike direction of approximately 45°. Eventually, we rotated the data accordingly prior to the inversion.

The 2D inversion algorithm after Rodi and Mackie (2001) was used to fit the MT data of both polarisations, representing electrical current systems parallel (E-polarisation) and perpendicular (B-polarisation) to the strike direction of the conductive structures of the subsurface. The regularization parameter t was set to 30

Table 2. Description of the samples attained from the South African Borehole Library in Pretoria for further examination. The second column gives the results of the impedance spectroscopy measurements; see Table 3 for details. Par. /perp.: measurements were taken parallel/perpendicular to the bedding of the sample.

Sample	Resistivity Ωm (min)	Resistivity Ωm (max)	Formation	Depth (m)	ID	Lithology
A	4	6	Whitehill	2789	9	Laminated fragile black shale. Trace pyrite and Fe-oxidation along fabric (Figure 3a).
B	363	4917	Prince Albert	2817	8	Laminated black shale. Pervasive irregular calcite veins (Figure 3b).
C (par.)	0.008	1710	Prince Albert	2863	1	Massive black-grey mudrock. One thick pyritic stringer (Figure 3c).
C (perp.)	46	322				
D (par.)	485	808	Prince Albert	2874	6	Homogenous, massive black-grey mudrock (Figure 3d).
D (perp.)	447	805				

after computing an L-curve, trading-off misfit against roughness. For the inversion, emphasis was placed on fitting the MT phases, setting an error floor of 0.6°, whereas the apparent resistivities of the E-polarisation data was down-weighted (error floor 100%) to avoid problems with static shift effects. The error floor of the B-polarisation apparent resistivities was set to 5%. With these settings, the inversion of MT3, as shown in Figure 2, achieved an rms misfit of 2.1. Clearly, with the limited data set this model must be taken as preliminary; we blanked areas where we cannot be certain how well structures are resolved.

However, the existence and the position of the sub-horizontal high conductivity band are well resolved. This conductive layer can be traced from the southern end of profile MT1 almost 200 km further to the northeast. From a depth of more than 5 km in the south, the layer becomes continuously shallower towards the northeast and outcrops in the vicinity of Vosburg. The resistivities of this layer along profiles MT1 and MT3 are in the order of 1 to 4 Ωm with an average thickness of approximately 300 - 500 m. Modelling studies based on the inclusion of tear zones in the inversion along profile MT4, 350 km further to the east, indicate that this layer can be much thinner (~100 m) if lower resistivities (0.3 Ωm) are assumed (Weckmann *et al.*, 2007b).

In summary, the MT data reveal a continuous, conductive layer - probably associated with the Whitehill Formation – that can be traced throughout the entire Karoo Basin in a north to south direction and possibly for another 350 km towards the east.

Vitrinite reflectance and organic petrography

Vitrinite reflectance (VR) analysis is a standard technique to determine the thermal maturity of organic matter in rocks. It is also an appropriate parameter to monitor the graphitization process, which is characterized by a strong increase in maximum vitrinite reflectance (Rmax) and in bireflectance (Rmax-Rmin; *e.g.* Stach *et al.*, 1982). The borehole SA1/66 (see Figure 1) was drilled by the Geological Survey of South Africa and deepened by SOEKOR in 1966 on the farm Sambokkraal. For this borehole, Cole and McLachlan (1994) reported organic carbon readings for the Whitehill and Prince Albert Formations, on average 4.9% total C_{Org} (based on 12 readings) for the Whitehill and 4.6% total C_{Org} (based on 3 readings) for the Prince Albert Formation. Figure 3 shows the four samples from SA1/66 taken from the South African Borehole Library, Pretoria. They cover a depth range from 2789 m to 2874 m (Table 2) and represent rocks from the Whitehill Formation (sample A) and the underlying Prince Albert Formation (samples B, C, and D). Rocks from the Prince Albert Formation vary in lithology between black shales with calcite veins to competent mudrocks with and without pyrite lenses.

Polished blocks were prepared from each sample parallel and perpendicular to the borehole axis. Maximum (Rmax) and minimum reflectance (Rmin) was measured on organic particles using a Leitz MPV microscope and established procedures (polarized light with a wavelength of 546 nm; immersion oil with a refractive index of 1.518; see Stach *et al.*, 1982). Organic matter in sample C, characterized by large idiomorphic pyrite crystals, is generally rare and organic particles are

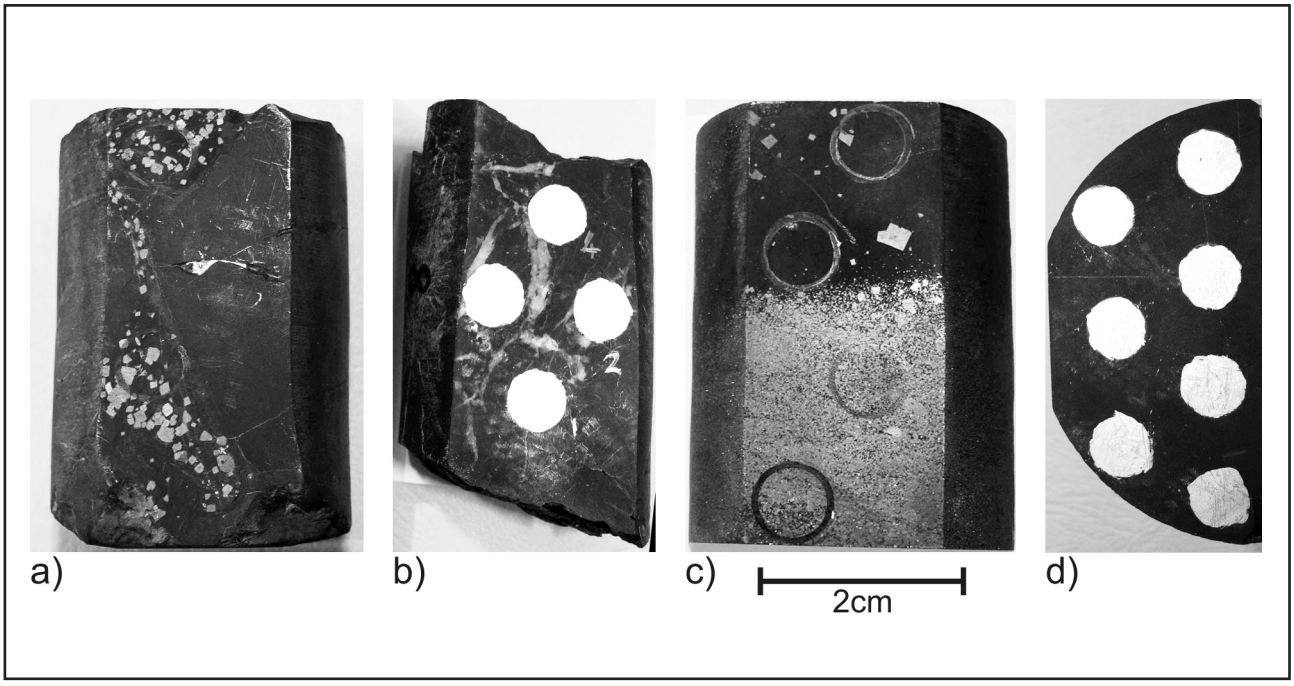

Figure 3. (**a**) Sample A from the Whitehill Formation with associated accessory pyrite restricted to one side of a rock fracture. (**b**) Sample B: pervasive calcite veins are clearly evident. (**c**) Sample C: the high proportion of pyrite is present in the lower portion of the sample. (**d**) Sample D is homogenous black shale. Platinum paint disks are still present on samples B and D. Samples B, C, and D are from the Prince Albert Formation.

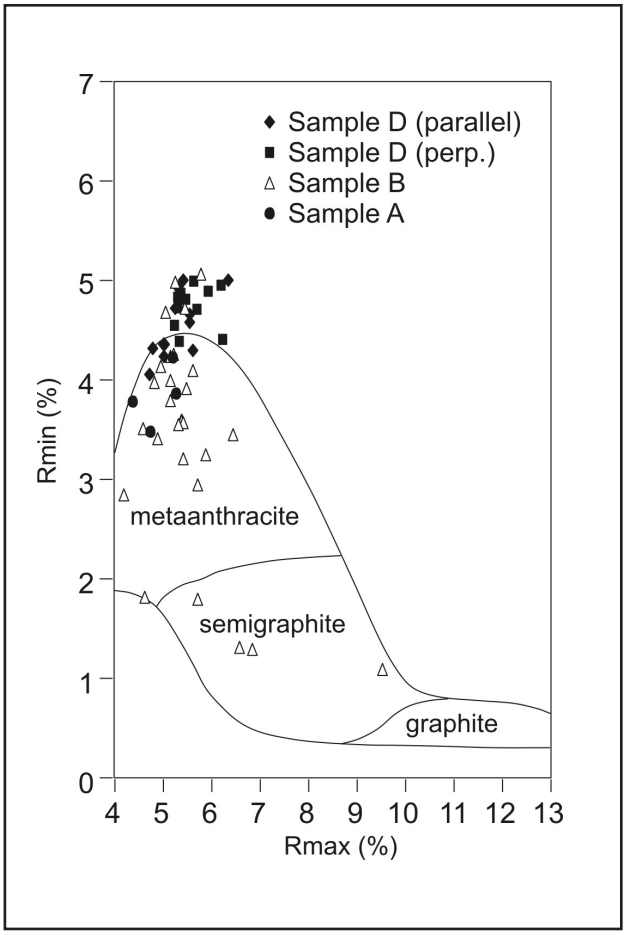

Figure 4. Reflectance of organic matter in borehole SA1/66. The outlined fields correspond to the reflectance of metamorphosed vitrinite according to Teichmüller *et al.* (1979).

always very small. Therefore, it was impossible to measure VR. Figure 4 shows a plot of maximum versus minimum reflectance of the other three samples.

Sample A contains fine-grained and coarse-grained parts. Distinct organic-rich layers occur within the fine-grained part. Rmax values range from 4.4% to 5.3% and Rmin values range from 3.5% to 4.7%. Particles with a high bireflectance are very rare. Solid bitumen occurs along bedding planes and fills fractures in the fine-grained part, but pore-coating solid bitumen is especially abundant in the more coarse-grained part. There is no major difference between the reflectance values of vitrinite and solid bitumen, although vitrinite tends to have lower Rmin values than solid bitumen.

Sample B is unique because it contains organic matter with both low and high bireflectance ("graphitic particles"), as indicated by the very wide range from metaanthracite to semigraphite (Figure 4). The "graphitic particles" usually have a fine anisotropic mosaic texture. Because of the mosaic texture and because they are generally very thin it was difficult to determine the "true" reflectance. Most probably, the bireflectance of some particles is even higher than indicated in Figure 4.

Sample D contains relatively large vitrinite particles. Rmax is about 5.5% to 6.0%, with a maximum value of 6.4%. Rmin values depend on the orientation of the polished block. Whereas it is 4.0% to 5.0% in a section parallel to the axis of the core, it is 4.4% to 5.0% in the block cut perpendicular to the core axis. In any case, both Rmax and Rmin are slightly higher than in sample A.

Based on the Rmax values, the organic matter in borehole SA1/66 is classified as metaanthracite. Rmin values are relatively high for this rank and hence bireflectance is relatively low. Bireflectance is known to be influenced by pressure conditions (*e.g.* Mastalerz *et al.*, 1993; Ross and Bustin, 1997). The low bireflectance could therefore result from Permian intermittent tectonic activity (see Table 1) and the Karoo's relatively shallow burial. Eagle *et al.* (1996) found temperatures never much above 200° C with pressures between 1 and 2 kbar, except for local hot spots in the Karoo Basin where some of the uranium deposits have been remobilized. However, effects due to different orientations of the polished surfaces cannot be excluded. Only sample B from the Prince Albert Formation contains significant amounts of particles with high bireflectance ("graphitic particles") together with organic matter with a low bireflectance (Figure 4). Slightly lower reflectance values in sample A compared to sample D may indicate increasing maturity with depth.

The co-existence of several types of carbonaceous matter that differ in their morphology, texture and reflectance is typical for rocks in the temperature range of 250 to 350ºC (*e.g.* Diessel *et al.*, 1978; Kribek *et al.*, 1994), which is in general agreement with the metamorphic range of the Karoo Basin. The differences in the degree of graphitization are traditionally attributed to the initial nature of the organic matter (*e.g.* vitrinite with a low bireflectance vs. liptinite with a high bireflectance). However, "graphitic particles" may also be produced by increased amounts of shear stress within this horizon (*e.g.* Nover *et al.*, 2005). Graphite can also be from the reduction of CH_4 and CO_2 released from thermal alteration and cracking of both kerogen and bitumen which (depending on the temperature, pressure, and oxygen fugacity) can be oxidized or reduced to form graphite (Kribek *et al.*, 1994).

The differences in the degree of graphitization in these samples represent a two-fold relation between initial composition of the carbonaceous matter and the nature and degree of the metamorphism, which may vary microscopically, taking into account hydrothermal effects and compositional changes. The relation to electrical conductivity is tentative as sample A from the Whitehill Formation, with a lower degree of graphitisation, yields higher conductivities than sample B (see section 5). However, efficient electrical conduction in sample A could be achieved by interconnection of microscopic graphite films at the grain boundaries. This was the case for high electrical

conductivities of black shales from the Münsterland-1 borehole where grain-boundary carbon was deposited during pyrolisis of organic carbon (Duba *et al.*, 1988).

Apart from the primary organic matter, solid bitumen is a common constituent in most samples. It is especially enriched in sample A where it is concentrated along bedding planes, fills fractures or coats pores in coarse-grained material. Solid bitumen has also been described from the Whitehill Formation by Cole and McLachlan (1994).

Impedance spectroscopy (IS)

Impedance spectroscopy is used to measure a rock sample's complex electrical impedance (*Z*). By measuring the phase shift between an applied oscillating potential difference and the measured current across a sample, the method identifies both the sample's resistivity and dielectric properties (Barsoukov and MacDonald, 2005). Out of phase polarization of bound charges within the applied oscillating fields results in a charge accumulation at grain boundaries and electrodes. Such dielectric effects are strongly dependant on the microstructure, porosity and composition of the sample (Guegen and Palciauskas, 1994). At higher frequencies this results in an energy loss which reaches a maximum at the resonant / critical frequency, $\omega=1/\tau$ where ω is the field's angular frequency and τ defines the relaxation time of the polarized bound charges. This capacitive effect is incorporated into the imaginary part of Z while at frequencies approaching that of direct currents the sample's bulk conductivity can be obtained from the real part of Z. The bulk properties, grain boundary behaviour and electrode polarizations can be separated by their differing time constants.

The complex frequency response of a rock sample can be interpreted in terms of an analogous electrical circuit (Guegen and Palciauskas, 1994), composed of a capacitor C in parallel with a resistor R (with conductance G=1/R) and driven by an oscillating voltage $V \sim e^{i\omega t}$. In a "Cole-Cole" diagram, the Im(*Z*) is plotted over the Re(Z). The data points should form a semi-circle with radius R, centred on the Re(*Z*) axis, while the Im(Z) is at maximum at the resonant/critical frequency. For the lowest frequencies, the imaginary part of Z becomes 0. The bulk resistivity of a sample is then calculated at Z_0 ($\omega>0$) as a function of the geometry of the sample if electrode polarizations can be neglected:

$$\rho_{rock} = Z_0 \cdot \frac{A}{l}[\Omega m],$$

A being the surface area, *l* the length of the sample.

To prepare the rock samples for IS, they were cut and ground to obtain parallel sides. Samples were then aerated for a month to dry the ground surfaces. Eventually, circular patches of platinum paint were applied to the samples using a stencil of 0.8 cm diameter at 0.5 cm spacing (see Figure 3). These platinum paint electrodes optimize connection with the sample's surface area by decreasing the polarization effects of the electrode-sample interfaces and delimit a specific surface area from which the bulk conductivity is obtained. Depending on the size of the sample, up to seven different positions to place the electrodes are possible on one side. Electrodes were connected to the platinum locations with a rubber sealed clamp. The data were measured with a BAS Zahner IMP6 potentiostat and analyzed using the Thales software package (http://www.bioanalytical.com/products/ec.html) at the GeoForschungsZentrum.

The experiments were conducted in a two-pole arrangement. However, four terminals were connected to the sample through the potentiostat which contains a control loop to maintain a constant stimulus voltage for the frequency response analyzer. The current was provided to the sample through a counter electrode and the output current was measured by a working electrode while two reference electrodes measured the potential difference between the poles.

Results of the IS for the samples of borehole SA1/66 are summarized in Table 2 and shown for individual samples and electrode configurations in Figure 5; further details of the IS measurements are given in Table 3. For most of the samples and electrode combinations a complete impedance arc could not be obtained by the measurements. This effect is caused by high impedances of the samples at a specific electrode point and related electrode effects at lower frequencies. However, extrapolated values for Z_0 can be computed based on an idealized, simple RC-model if the high frequency part of the impedance data are used (solid lines in the diagrams of Figure 5). For the rock samples of the Prince Albert Formation (samples B, C, and D), resistivities vary tremendously between 4917 Ωm and 0.008 Ωm. One recording of sample C, in particular, reveals exceptional conductivity values. For measurements taken through a pyrite stringer (Figure 3c; bottom portion of the sample) the sample responded almost like a perfect (metallic) conductor. When measurements were taken on pyrite free portions, the measured rock resistivity values were very high (> 1000 Ωm).

Sample B also exhibits a broad range of bulk resistivities of between 363 Ωm and 4917 Ωm. This broad range can be explained by the pervasive calcite veining that is dominant throughout the sample (Figure 3b). These calcite veins prevent charge transport across the sample. This infilling of laterally extensive cracks with calcite noticeably destroys secondary porosity and was described in borehole KW1/67 (SOEKOR KW1/67). For one recording on sample B we managed to set the electrode points avoiding the resistive calcite veins; the resulting resistivities are intermediate at 363 Ωm.

For sample A from the Whitehill Formation the readings were more consistent and Z_0 could be

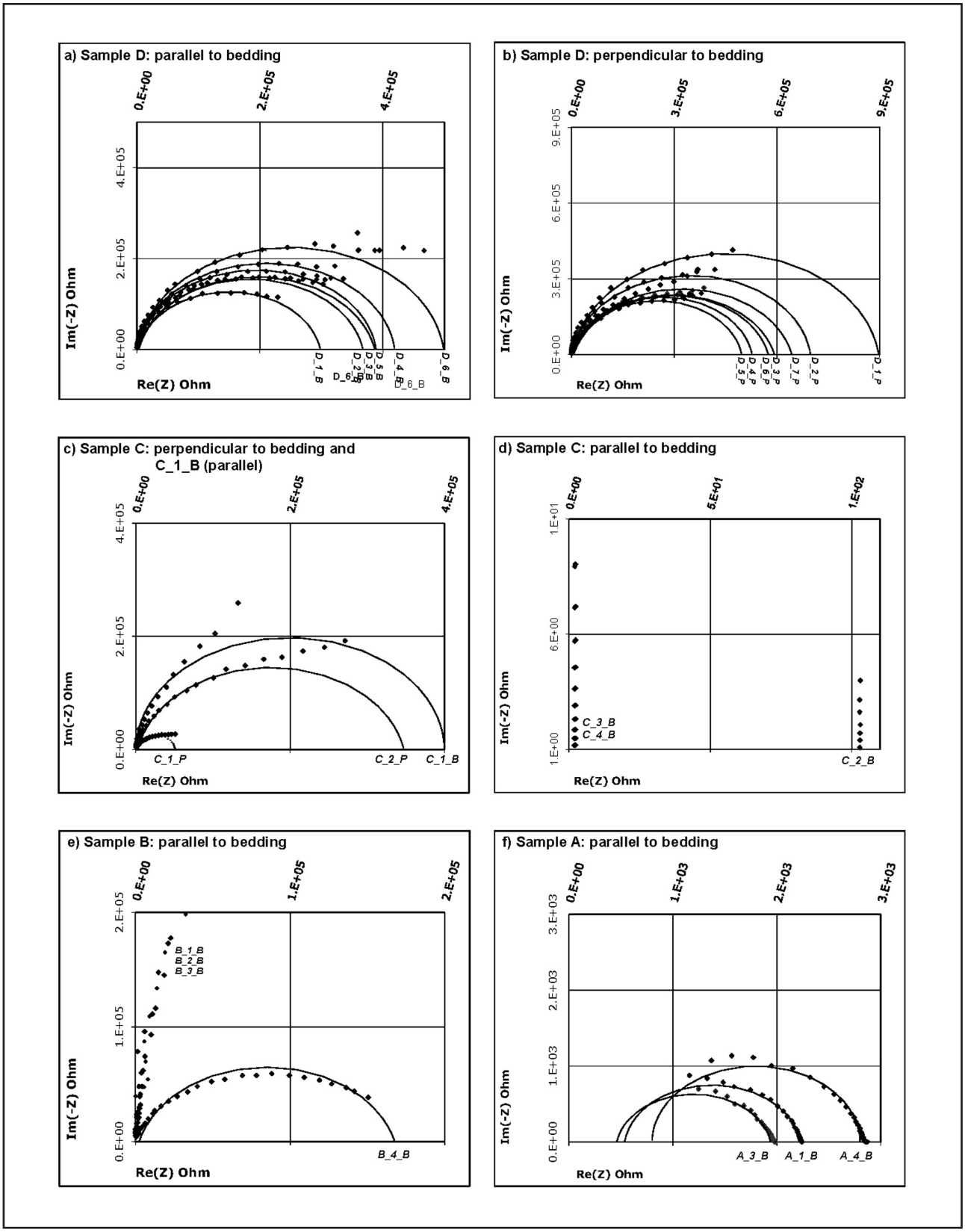

Figure 5. Impedance Z plotted as a "Cole-Cole" diagram. Solid lines represent a RC- model to fit the measured data (black diamonds). The bulk resistivity of a rock sample is calculated from the low frequency (or DC) impedance Z_0 (see text). Sample D in (**a**) and (**b**) shows consistently high impedance values with a bulk rock resistivity varying between approximately 450 Ωm and 800 Ωm (see also Table 2). Sample C in (**c**) and (**d**) shows immensely varying conductivities, ranging over 5 orders of magnitude. The high conductivity is largely controlled by the presence of a pyritic-rich stringer. Sample B in (**e**) indicates high resistivity, probably caused by the presence of calcite veins. In one of the readings with lower resistivity values, these calcite veins may have been avoided. Sample A from the Whitehill Formation in (**f**) has consistently low resistivities on the order of 5 Ωm.

Table 3. Details of the impedance spectroscopy measurements: listed above are the results of electrical conductivity measurements of the borehole samples for various electrode combinations. The samples, together with the platinum paint electrodes are shown in Figure 3.

	Reading	**Zre (Ω)**	**Resistivity Ωm**			
Sample C	C_1_B*	4.00E+05*	1.71E+03*	427.7	Average	Ωm
(= to bed)	C_2_B	1.03E+02	4.40E-01	1710.4	Max	
	C_3_B	1.90E+00	8.12E-03	0.008	Min	
	C_4_B	2.30E+00	9.83E-03	855.1	Standard deviation	
				n=4		
Sample C	C_1_P	5.00E+04	4.60E+01	184.1	Average	Ωm
(⊥to bed)	C_2_P	3.50E+05	3.22E+02	322.2	Max	
				46.0	Min	
				195.3	Standard deviation	
				n=2		
			Sample C	346.5	Average	Ωm
			All readings	1710.4	Max	
				0.008	Min	
				679.9	Standard deviation	
				n=6		
Sample D	D_1_B	3.00E+05	4.85E+02	637.4	Average	Ωm
(⊥to bed)	D_2_B	3.65E+05	5.90E+02	808.5	Max	
	D_3_B	3.90E+05	6.31E+02	485.1	Min	
	D_4_B	4.20E+05	6.79E+02	106.3	Standard deviation	
	D_5_B	3.90E+05	6.31E+02	n=6		
	D_6_B	5.00E+05	8.08E+02			
Sample D	D_1_P	9.00E+05	8.05E+02	568.3	Average	Ωm
(= to bed)	D_2_P	7.00E+05	6.26E+02	805.5	Max	
	D_3_P	6.00E+05	5.37E+02	447.5	Min	
	D_4_P	5.20E+05	4.65E+02	121.3	Standard deviation	
	D_5_P	5.00E+05	4.47E+02	n=7		
	D_6_P	5.80E+05	5.19E+02			
	D_7_P	6.45E+05	5.77E+02			
			Sample D	600.2	Average	Ωm
			All readings	808.5	Max	
				447.5	Min	
				115.6	Standard deviation	
				n=13		
Sample B	B_1_B	2.00E+06	4.28E+03	3511.7	Average	Ωm
(= to bed)	B_2_B	2.10E+06	4.49E+03	4917.5	Max	
	B_3_B	2.30E+06	4.92E+03	363.5	Min	
	B_4_B	1.70E+05	3.63E+02	2115.7	Standard deviation	
				n=4		
Sample A	A_1_B	2.25E+03	4.81E+00	5.1	Average	Ωm
(= to bed)	A_3_B	2.00E+03	4.28E+00	6.2	Max	
	A_4_B	2.90E+03	6.20E+00	4.3	Min	
				1.0	Standard deviation	
				n=3		

determined for all recordings; the observed resistivities are low, varying between 4 Ωm to 6 Ωm.

Discussion and conclusions

Already Duba *et al.* (1988; 1994) pointed out that pyrite can be an effective contributor to electronic conduction. From sample C we can see clearly that if interconnected, the pyrite is significantly lowering the bulk resistivity. The picture is less clear in our samples where carbon is the dominant phase. For rock sample A from the Whitehill Formation the observed conductivity was consistently high, while generally low conductivities were obtained for sample B. This is unexpected because sample B contains a higher amount of "graphitic particles" which are known to be good electrical conductors. In fact, many of the high conductivity anomalies found with MT studies in tectonically inactive regions have been attributed to the existence of graphite (*e.g.* Ritter *et al.*, 1999; Tauber *et al.*, 2003; Pous *et al.*, 2004). In sample A the organic matter is often enriched

in distinct organic-rich layers, which could increase the connectivity of the graphite crystals and thereby increase the bulk electrical conductivity. Alternatively, the interconnection needed for efficient electrical conduction could be related to the deposition of fine-grained kerogen and solid bitumen at grain boundaries between highly conductive graphite crystals within the previously porous laminae of sample A. This seems plausible considering the nature of the pyrite in this sample, which appears to have formed by fluid flow (Figure 3a). Such hydrothermally driven events are well documented for the Karoo Basin (Duane and Brown, 1992; McDonald and Rozendaal, 1995) and its uranium deposits (Duane *et al*., 1989). The organic petrological data for sample A would support this hypothesis and is consistent with the observations of Duba *et al*. (1988).

Even if the rocks appear to have low porosity, decompression and drying of the samples may have led to higher grain boundary resistivities due to an increase of pressure release induced micro-cracks. Therefore, the measured conductivities of the rock samples represent a minimum conductivity of the formations. Judging from perturbation estimates (Bahr, 1997; Weidenfeller *et al*., 2002) an extremely high pyrite fraction would be required to sustain an interconnected network of pyrite within the Prince Albert Formation. Small clusters of pyrite – as observed in the drill cores – enhance the electrical conductivity only locally. Jones *et al*. (1997) discuss that pyrite in fold-hinges could partly be responsible for the North American Central Plain conductivity anomaly. However, given the huge areal extend of the observed MT conductivity anomaly, it seems more plausible, to attribute the cause of the anomaly to another stratigraphic unit. The high average conductivity of 4 to 6 Ωm of the Whilehill Formation seems better suited to explain the observations.

In summary, it is plausible that the sub-horizontal conductivity anomaly in the MT model is at least partly caused by the transgressive, fine-grained, carbon-rich sequences of the Whitehill Formation. However, the lower Prince Alfred Formation with similarly gradational composition changes, especially regarding carbon content (Cole and McLachlan, 1994), cannot be excluded as an additional contributor. Constrained inversions of the MT data show that the high conductivity layer associated with the Whitehill Formation must be horizontally continuous. The best resolved parameter of a layered conductor in any MT model is the product of the layer's thickness and its conductivity, the so-called integrated conductance. The model in Figure 2 reveals an integrated conductance (in excess) of 300 S, if we assume an average thickness of 300 m with a resistivity of around 1 Ωm for the Whitehill Formation. If resistivities are as low as 0.3 Ωm, as discussed in Weckmann *et al*. (2007b), this would lead to a layer thickness of 100m, more in line with the average thickness reported for the Whitehill Formation of 50 m to 70 m. Either way, the MT models suggest that this highly conductive layer is more or less continuously extending throughout the entire Karoo Basin except for the southernmost portion of the basin where a duplication of the sequences is documented (Newton, 1992). The high conductivity layer is also present in a profile crossing the Beattie Magnetic Anomaly some 350 km further to the west of the main profiles (see Figure 1 and Weckmann *et al*., 2007b). This would make the high conductivity layer an effective marker horizon for the lower Karoo (Ecca Group) and, by taking the thickness of the underlying Dwayka Formation into account, an indirect marker to the top of the Namaqua basement.

Acknowledgements

TB was generously supported by the GFZ Potsdam. UW was funded by the Emmy Noether fellowship of the German Science Foundation (DFG). The MT instruments for the experiments were provided by the Geophysical Instrument Pool Potsdam. The field and laboratory experiments were funded by the GFZ Potsdam. We thank Brian Horsfield (GFZ) for initiating the VR analyses. We are grateful for helpful comments in reviews by Maarten de Wit (editor), Arne Hoffmann-Rothe, and A.G. Jones. We would like to sincerely thank Maarten de Wit and Brian Horsfield for all the hard work they put into Inkaba yeAfrica, including this special volume of South African Journal of Geology. This is Inkaba yeAfrica contribution number 16.

References

Bahr K. (1997). Electrical anisotropy and conductivity distribution functions of fractal random networks and of the crust: the scale effect of connectivity. *Geophysical Journal International*, **130**, 649–660.

Barsoukov E. and Macdonald J.R. (Editors) (2005). Impedance Spectroscopy Theory, Experiment and Applications. *John Wiley and Sons, New York, United States of America,* 616pp.

Catuneanu O. (2004). Basement control on flexural profiles and the distribution of foreland facies: The Dwyka Group of the Karoo Basin. *South Africa, Geology*, **32**, 517-520.

Cole D.I. (1992). Evolution and development of the Karoo Basin, *In:* M.J. de Wit and I.D.G. Ransome (Editors) Inversion tectonics of the Cape Fold Belt. Karoo and Cretaceous Basins of Southern Africa*, A. A. Balkema, Rotterdam, The Netherlands*, 87-100.

Cole D.I. and McLachlan I.R. (1994). Oil shale potential and depositional environment of the Whitehill Formation in the main Karoo Basin. *SOEKOR, now PASA, South African Petroleum Agengy, Cape Town. Unpublished Report No. 1994-0213.*

Craddock J.P., McKiernan A.W., de Wit M.J. (2007). Calcite twin analysis in syntectonic calcite, Cape Fold Belt, South Africa: Implications for fold and cleavage formation within a shallow thrust front. *Journal of Structural Geology,* **29**, 1100-1113.

de Beer J., van Zijl J. and Gough D. (1982). The Southern Cape Conductive Belt (South Africa): Its Composition, Origin and Tectonic Significance. *Tectonophysics*, **83**, 205-225.

Diessel C.F.K., Brothers R.N. and Black P.M. (1978). Coalification and graphitization in high-pressure schists in New Caledonia. *Contributions to Mineralogy and Petrology*, **68**, 63-78.

Duane M.J., Welke H.J. Allsopp H.L. and Wilsher W.A. (1989). U-Pb isotope systematics, ages and genesis of Karoo uranium deposits, South Africa. *South African Journal of Geology*, **92**, 49-64.

Duane M.J. and Brown R. (1992). Geochemical open-system behaviour related to fluid-flow and metamorphism in the Karoo. *In:* M.J. de Wit and I.G.D. Ransome (Editors), Inversion tectonics of the Cape Fold Belt, Karoo and Cretaceous Basins of Southern Africa*, Balkema, Rotterdam, The*

Netherlands, 127-140.

Duba A., Heikamp S., Meurer W., Nover G. and Will G. (1994). Evidence from borehole samples for the role of accessory minerals in lower-crustal conductivity. *Nature*, **367**, 59-61.

Duba A., Huenges E., Nover G. and Will G. (1988). Impedance of black shale from Munsterland 1 borehole: an anomalously good conductor. *Geophysical Journal*, **94**, 413-419.

Egle S. (1996). Paleohydrology of the Cape fold belt and Karoo Basin, South Africa. *Unpublished PhD thesis, University of Cape Town, South Africa*, 155pp.

Egle S., de Wit M.J., Hoernes S. (1998). Gondwana fluids and subsurface palaeohydrology of the Cape Fold belt and the Karoo Basin, South Africa. *Journal of African Earth Sciences*, **27**, 63-64.

Gough D.I., de Beer J.H. and van Zijl J.S.V. (1973). A magnetometer array in Southern Africa. *Geophysical Journal of the Royal Astronomical Society*, **34**, 421-433.

Guegen Y. and Palciauskas V. (1994). Introduction to Physics of Rocks. *Princeton University Press, Princeton, New Jersey, U.S.A.*, 294p.

Halbich I.W. (1983). *In:* A.O.G. Sohnge and I.W. Halbich (Editors). A tectogenesis of the Cape Belt (CBF). Geodynamics of the Cape Fold Belt, *The Geological Society of South Africa Special Publication,* **12**, 165-175.

Halbich I.W. (1992). The Cape Fold Belt Orogeny: State of the art 1970s-1980s. *In:* M.J. de Wit and I.D.G. Ransome (Editors) Inversion tectonics of the Cape Fold Belt, Karoo and Cretaceous Basins of Southern Africa*, A. A. Balkema, Rotterdam, The Netherlands*, 141-158.

Johnson M.R., van Vuuren C.J., Hegenberger W.F., Key R. and Shoko U. (1996). Stratigraphy of the Karoo Supergroup in South Africa: an overview. *Journal of African Earth Science*, **23**, 3-15.

Kribek B., Hrabal J., Landais P. and Hladikova J. (1994). The association of poorly ordered graphite, coke and bitumens in greenschist facies rocks of the Ponikl Group, Lugicum, Czech Republic: the results of graphitization of various types of carbonaceous matter. *Journal of Metamorphic Geology*, **12**, 493-503.

Lopez-Gamudi O.R. and Rossello E.A. (1998). Basin fill evolution and paleotectonic patterns along the Samfrau geosyncline: the Sauce Grande basin-Ventana foldbelt (Argentina) and Karoo basin-Cape foldbelt (South Africa) revisited. *Geologische Rundschau*, **86**, 819-834.

Mastalerz M., Wilks K. R., Bustin R. M. and Ross J. V. (1993). The effect of temperature, pressure and strain on carbonization in high-volatile bituminous and anthracitic coals. *Organic Geochemistry*, **20**, 315-325.

McDonald W.G. and Rozendaal A. (1995). The Geelwal Karoo heavy mineral deposit: a modern day beach placer. *Journal of African Earth Science*, **21**, 187-200.

Milani E.J. and de Wit M.J. (2007). Correlations between the classic Paraná and Cape-Karoo sequences of South America and southern Africa and their basin infills flanking the Gondwanides: Du Toit revisited. *In:* R. Pankhurst et al. (Editors), Western Gondwana - the Ties that Bind. *The Geological Society, London,* (in press).

Newton A.R. (1992). Thrusting on the northern margin of the Cape Fold Belt, near Laingsburg. *In:* M.J. de Wit and I.D.G. Ransome (Editors) Inversion tectonics of the Cape Fold Belt, Karoo and Cretaceous Basins of Southern Africa*, A. A. Balkema, Rotterdam, The Netherlands*, 193-196.

Nover G., Stoll J.B. and von der Gönna, J. (2005). Promotion of graphite formation by tectonic stress - a laboratory experiment. *Geophysical Journal International*, **160 (3)**, 1059–1067, doi:10.1111/j.1365-246X.2005.02395.x.

Pous J., Munoz G., Heise W., Melgarejo J.C. and Quesada C. (2004). Electromagnetic imaging of Variscan crustal structures in southwest Iberia: the role of interconnected graphite. *Earth and Planetary Science Letters*, **217**, 435–450.

Ritter O., Haak V., Rath V., Stein E. and Stiller M. (1999). Very high electrical conductivity beneath the Münchberg Gneiss area in Southern Germany: implications for horizontal transport along shear planes. *Geophysical Journal International*, **139**, 161–170, doi:10.1046/j.1365-246X.1999.00937.x.

Rodi W. and Mackie R. L. (2001). Nonlinear conjugate gradients algorithm for 2D magnetotelluric inversion. *Geophysics*, **66**, 174-187.

Ross J.V. and Bustin R.M. (1997). Vitrinite anisotropy resulting from simple shear experiments at high temperature and high confining pressure. *International Journal of Coal Geology*, **33**, 153-168.

Snymann C.P (1998). Coal. *In:* M.G.C. Wilson and C.R. Anhaeusser (Editors), The Mineral Resources of South Africa *Council for Geoscience, South Africa*, *Handbook*, **16**, 136-205.

SOEKOR FILE CR1/68, CR 1/68. *Borehole Master Report Log, Open File report, Council for Geoscience library, Pretoria, South Africa*.

SOEKOR FILE KW1/67, KW1/67. *Borehole Master Report Log, Open File report, Council for Geoscience library, Pretoria, South Africa*.

Stach E., Taylor G.H., Mackowsky M.-Th., Chandra D., Teichmüller M., and Teichmüller R. (1982). Stach's Textbook of Coal Petrology. 3rd Edition, *Gebrüder Bornträger, Berlin, Germany*, 535p.

Tauber S., Banks R., Ritter O. and Weckmann U. (2003). A high-resolution magnetotelluric survey of the Iapetus Suture Zone in southwest Scotland. *Geophysical Journal International*, **153**, 548–568, doi:10.1046/j.1365-246X.2003.01912.x.

Teichmüller M., Teichmüller R. and Weber M. (1979). Inkohlung und Illit-Kristallinität (Vergleichende Untersuchungen im Mesozoikum und Paläozoikum von Westfalen). *Fortschritte der Geologie Rheinland und Westfalen*, **27**, 201-276.

Van Zijl J.S.V. (2006). A review of the resistivity structure of the Karoo Supergroup, South Africa, with emphasis on the dolerites: A study in anisotropy. *South African Journal of Geology*, **109**, 315-328.

Weckmann U., Ritter O., Jung A., Branch T. and de Wit M. (2007a). Magnetotelluric measurements across the Beattie magnetic anomaly and the Southern Cape Conductive Belt, South Africa. *Journal of Geophysical Research*, **112**, B05416, doi:10.1029/2005JB003975.

Weckmann U., Jung A., Branch T. and Ritter O. (2007b). Comparison of electrical conductivity structures and 2D magnetic modelling along two profiles crossing the Beattie Magnetic Anomaly, South Africa. *South African Journal of Geology*, **110**, 449-464.

Weidenfeller B., Höfer M. and Schilling F. (2002). Thermal and electrical properties of magnetite filled polymers. *Composites: Part A*, **33**, 1041–1053.

Editorial handling: M.J. de Wit and Brian Horsfield